

High sensitivity absorption spectroscopy of methane at 80 K in the 1.58 μm transparency window: Temperature dependence and importance of the CH_3D contribution

L. Wang^a, S. Kassi^a, A.W. Liu^{a,b}, S.M. Hu^b, A. Campargue^{a,*}

^aLaboratoire de Spectrométrie Physique (associated with CNRS, UMR 5588), Université Joseph Fourier de Grenoble, B.P. 87, 38402 Saint-Martin-d'Hères Cedex, France

^bHefei National Laboratory for Physical Sciences at Microscale, University of Science and Technology of China, Hefei 230026, China

ARTICLE INFO

Article history:

Received 13 January 2010

In revised form 19 February 2010

Available online 3 March 2010

Keywords:

Methane

CH_4

CH_3D

Titan

Absorption spectroscopy

Cryogenic cell

CRDS

HITRAN

ABSTRACT

The high resolution absorption spectrum of methane in the 1.58 μm transparency window has been recorded at room temperature and at 79 K by CW-Cavity Ring Down Spectroscopy using a cryogenic cell and a series of Distributed Feed Back (DFB) diode lasers. The achieved sensitivity ($\alpha_{\text{min}} \sim 3 \times 10^{-10} \text{ cm}^{-1}$) has allowed for a detailed characterization of the 6289–6526 cm^{-1} region which corresponds to the lowest opacity of the transparency window. A list of 6868 and 4555 transitions with intensities as weak as $1 \times 10^{-29} \text{ cm}^2/\text{molecule}$ was constructed from the recordings at 297 and 79 K, respectively. By comparison with a spectrum of CH_3D recorded separately by Fourier Transform Spectroscopy, 1282 and 640 transitions of monodeuterated methane, CH_3D , in natural abundance in our sample were identified at 297 and 79 K, respectively.

The rotational temperature determined from the intensity distribution of the $3\nu_2$ band of CH_3D (79.3 K) was found in good agreement with the temperature value previously obtained from the Doppler line broadening. The reduction of the rotational congestion by cooling down to 79 K reveals a spectral region near 6300 cm^{-1} where CH_3D transitions are dominant.

The low energy values of the transitions observed both at 79 K and at room temperature were derived from the variation of their line intensities. These transitions with lower energy determination represent 93.9% and 68.4% of the total absorbance in the region, at 79 K and room temperature, respectively. The quality of the obtained empirical low energy values is demonstrated for CH_4 by the marked propensity of the empirical low J values to be close to integers. The line lists at 79 K and room temperature provided as Supplementary Material allow accounting for the temperature dependence of methane absorption between these two temperatures. The investigated region covering the $5\nu_4$ band of the $^{12}\text{CH}_4$ isotopologue will be valuable for the theoretical treatment of this band which is the lowest energy band of the icosad.

© 2010 Elsevier Inc. All rights reserved.

1. Introduction

The experimental characterization of the low temperature spectrum of methane in the spectral windows of low opacity is challenging as it supposes to combine a high sensitivity absorption technique with a cryogenic cell. Such laboratory measurements are nevertheless highly suitable because the transparency windows are used to analyze the deeper atmosphere of the giant outer planets and Titan and to infer the surface reflectivity with direct implications on its composition. For instance, Titan's atmosphere is roughly equivalent to a 20 km cell at $T = 85 \text{ K}$, containing N_2 at a pressure of 1.5 bar and approximately 75 mbar of CH_4 . In absence of accurate laboratory measurements, empirical bands models are

generally used by astronomers but they display important deficiencies in the transparency windows [1,2].

The present work is devoted to the first study of the 1.58 μm transparency window by highly sensitive absorption spectroscopy at low temperature. It is part of our recent systematic investigation of the temperature dependence of the absorption spectrum from room temperature (RT) to liquid nitrogen temperature (LNT), over the wide 1.26–1.71 μm region [3]. The two high absorbing regions surrounding the methane transparency window at 1.58 μm were characterized by differential absorption spectroscopy (DAS) at 81 K using a specifically designed cryogenic cell and a series of several tens Distributed Feed Back (DFB) diode lasers. This experimental approach provided a sufficient sensitivity ($\alpha_{\text{min}} \sim 10^{-6} \text{ cm}^{-1}$) in the high energy part of the tetradecad (5850–6180 cm^{-1}) [4,5] and in the icosad region (6700–7700 cm^{-1}) [6,7]. In the 1.58 μm transparency window corresponding to the 6180–6700 cm^{-1} gap, a higher

* Corresponding author.

E-mail address: Alain.Campargue@ujf-grenoble.fr (A. Campargue).

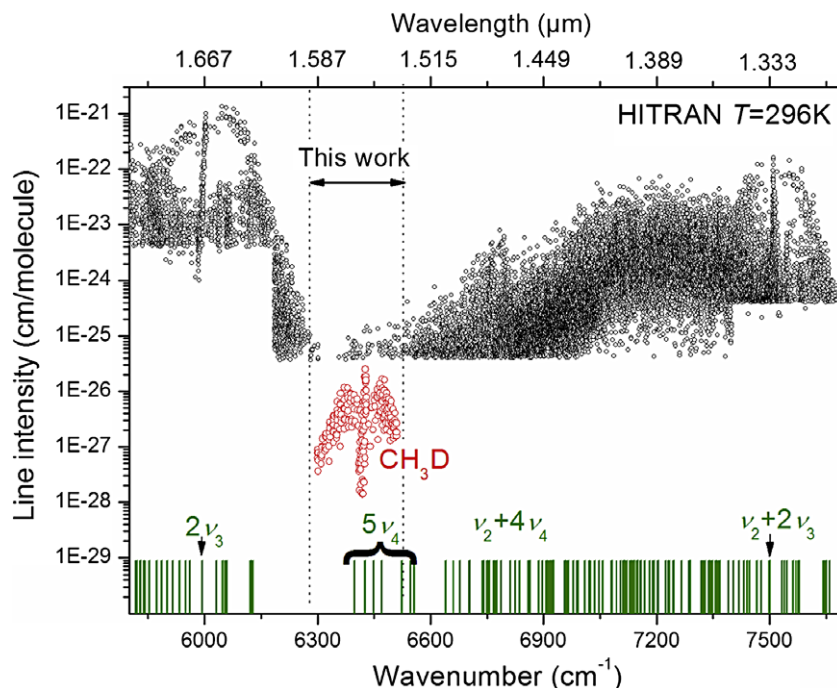


Fig. 1. Overview spectrum of methane at 296 K as provided in the HITRAN database for the 5800–7700 cm^{-1} region. It includes the $3\nu_2$ band of CH_3D with intensities scaled according to the natural abundance. The sticks at the bottom of the graph correspond to the centers of the $^{12}\text{CH}_4$ vibrational band predicted by Bowman et al. [19]. The rectangle marks the section of the 1.58 μm transparency window presently investigated.

sensitivity is required. We have recently been able to combine the CW-Cavity Ring Down Spectroscopy (CW-CRDS) technique with the same cryogenic cell [8]. The sensitivity achieved by CW-CRDS at both RT [9] and LNT [10] ($\alpha_{\min} \sim 3 \times 10^{-10} \text{ cm}^{-1}$) lowers by more than three orders of magnitude that of our DAS measurements.

It is well known that in the low opacity spectral regions, the relative contribution of the minor isotopologues to the absorption may largely exceed their relative abundance. This is the case for CH_3D in the considered 1.58 μm transparency window of methane. The D/H isotopic substitution leads to an important change of one stretching frequency, ν_2 , and the corresponding second overtone of CH_3D , $3\nu_2$, falls in the center of the CH_4 transparency window. This CH_3D band at 6430 cm^{-1} has been used to determine the D/H ratio in Saturn [10], Neptune [11], Uranus [12] and Titan [13]. Due to its particular interest in planetology, the $3\nu_2$ band has been the subject of several studies by Fourier Transform Spectroscopy (FTS): line positions and determination of the rotational constants [14], line intensities [15], pressure broadening and shift [16,17].

The overview spectrum of methane as provided in the HITRAN database at 296 K [18] is presented in Fig. 1 for the whole 1.26–1.71 μm region. From its last version, the $3\nu_2$ band of CH_3D has been included in the HITRAN line list of methane. The corresponding line intensities being multiplied by the relative abundance of CH_3D (6.15×10^{-4} [18]), it leads to values ranging between 4.3×10^{-27} and $2.5 \times 10^{-26} \text{ cm/molecule}$ i.e. below the $4 \times 10^{-26} \text{ cm/molecule}$ intensity cut off corresponding to the main isotopologue. The CH_3D absorption is then observed superimposed to the absorption of the main isotopologue which is poorly characterized at RT and practically unknown at low temperature. This is the reason why the analysis of the planetary atmospheres performed by de Bergh et al. [11–13] used Saturn spectrum as an intermediary spectrum of methane at low temperature. This was an important limitation of the method which contributed importantly to the uncertainty of the retrieved D/H ratios.

Our project is then to characterize the methane spectrum at low temperature in the region of the $3\nu_2$ band of CH_3D . The spectral section investigated ($6289\text{--}6526 \text{ cm}^{-1}$) is indicated in Fig. 1. In

the lower part of this figure, the vibrational band origins of $^{12}\text{CH}_4$ as calculated by Bowman et al. [19] are presented. From these calculations, it appears that the different components of the $5\nu_4$ band fall in the investigated region and are then the main responsible of the $^{12}\text{CH}_4$ absorption in the region. The $5\nu_4$ band is the lowest energy band of the icosad. This polyad remains without theoretical modeling apart from a partial analysis of the $\nu_2 + 2\nu_3$ band at the high energy opposite (7500 cm^{-1}). Being an “edge” vibrational band, the $5\nu_4$ band is expected to be less affected by the many rovibrational interactions perturbing the other bands of the polyad. The future theoretical analysis of the CRDS spectra of the $5\nu_4$ band will greatly benefit of the drastic reduction of the rotational congestion by cooling down to LNT.

The rest of this report is organized as follows: The CW-CRDS spectrometer and the spectral acquisition are described in Section 2. In Section 3, the construction of the line lists from the CW-CRDS spectra at LNT and RT is presented. This task was particularly laborious considering the complexity and congestion of the recorded spectra (about 20–30 lines per cm^{-1}). Section 4 is devoted to the identification of the CH_3D lines in the RT and LNT spectra by comparison with a spectrum of CH_3D at room temperature, recorded separately by Fourier Transform Spectroscopy. Then, we will present in Section 5, the determination of the low energy levels of the CH_4 and CH_3D transitions from the ratio of the line intensities retrieved from the CW-CRDS spectra at LNT and RT. The low energy levels are necessary to compute the Boltzmann factors which rule the temperature dependence of the line strengths and are valuable for the theoretical interpretation of the observed vibrational bands. Finally, the obtained results will be discussed in the last section and perspectives for future works will be presented (Section 6).

2. Experiment

2.1. CW-CRDS at room temperature

The CW-CRDS spectra at room temperature were recorded over the whole transparency window with our “standard” fibered DFB

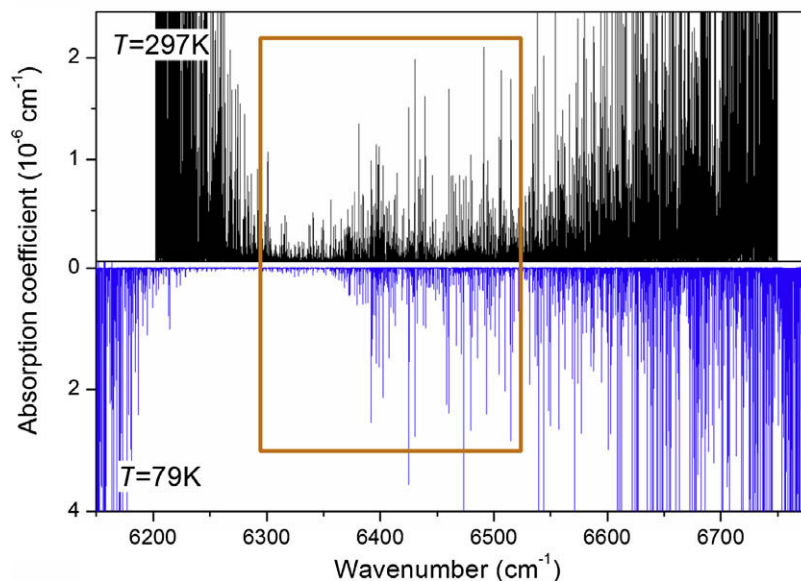


Fig. 2. Comparison of the CW-CRDS spectra of methane recorded at room temperature (upper panel) and liquid nitrogen room temperature (lower panel) in the 1.58 μm transparency window ($6150\text{--}6780\text{ cm}^{-1}$). The RT and LNT spectra correspond to 1.0 and 10.0 Torr, respectively. The rectangle marks the spectral section window presently investigated.

laser CW-CRDS spectrometer. The reader is referred to Refs. [9,20,21] for the description of the experimental apparatus. The $6165\text{--}6750\text{ cm}^{-1}$ region was continuously covered with the help of 27 fibered DFB lasers. The DFB typical tuning range is about 35 cm^{-1} by temperature variation from -5 to $60\text{ }^{\circ}\text{C}$. The stainless steel ring down cell ($l = 1.42\text{ m}$, $\Phi = 10\text{ mm}$) is fitted by a pair of super mirrors with a typical ring down time on the order of $\tau \sim 60\text{ }\mu\text{s}$. About 100 ring down events were averaged for each spectral data point, and about 60 min were needed to complete a temperature scan of one DFB laser. The corresponding noise equivalent absorption is on the order of $5 \times 10^{-10}\text{ cm}^{-1}$ [9].

2.2. CW-CRDS at LNT

The cryogenic cell specifically developed for CW-CRDS at low temperature has been described in Refs. [4,8]. Briefly, it is based on an original design (see Fig. 1 of Ref. [8]) which dispenses with an external vacuum jacket by exploiting the fact that a low pressure sample constitutes itself a good thermal insulation. The cryostat is a 1.42 m long hollow cylinder both filled and completely surrounded by the sample gas volume. The liquid nitrogen filling tube constitutes its single suspension point which, combined with an almost perfect cylindrical geometry helps to eliminate stress normally present in a double-jacket cell configuration. The distance between the high reflective mirrors and the cryostat ends is about 0.5 cm. As mentioned above, this cryogenic cell with the external cylinders fitted by a pair of flanges housing anti-reflection coated windows, is the one which was used to study the LNT absorption spectrum by differential absorption spectroscopy in the surrounding strong absorption regions [4–7].

To avoid possible difficulties due to operation at low temperature, the usual piezoelectric actuator that modulates the optical cavity length in standard CW-CRDS was not installed and a Mode by Mode CRDS acquisition scheme was preferred [8]. The two highly reflective mirrors were glued on hollow fingers which were themselves carefully glued on the cell flanges. The spectra were recorded using the same series of DFB lasers diodes than for the RT spectra except that there were extended down to 6150 cm^{-1} . A fast (200 Hz) triangular current modulation was applied to the DFB laser while its temperature was slowly ramped from -10 to $60\text{ }^{\circ}\text{C}$

within 1 h. This temperature ramp pulls the laser frequency over about 35 cm^{-1} . The current modulation leads to a frequency excursion of about 150 MHz, *i.e.* slightly more than the Free Spectral Range of our cavity (106 MHz). The average ring-down repetition rate was close to 500 Hz.

Using mirrors with 99.992% reflectivity, a noise equivalent absorption of $3 \times 10^{-10}\text{ cm}^{-1}$ was obtained for each spectral point on a 106 MHz grid. The achieved detection limit and dynamic range (4 decades) are then comparable to those obtained at RT.

During the recording of both the RT and LNT spectra, the pressure, measured by a capacitance gauge and the ring down cell temperature were monitored. The RT value was $297 \pm 2\text{ K}$ and most of the RT spectra were recorded at 2.5 and 10.0 Torr, as presented in Ref. [9]. Additional RT recordings were performed at 1.0 Torr in order to avoid saturation of the strongest transitions. The LNT spectra were recorded at 1.0, 5.0 and 10.0 Torr. The gas temperature in the cryogenic cell was calculated to be 82.6 K from the Doppler profile of several tens of lines [8]. We will present below a new determination of the gas temperature from the intensity distribution of the $3\nu_2$ band of CH_3D . The value of 79.3 K derived for the rotational temperature (Section 4) is what we refer to as “liquid nitrogen temperature” (LNT).

Each 35 cm^{-1} wide RT spectrum recorded with one DFB laser was calibrated independently on the basis of the wavelength values provided by the Michelson-type wavemeter (Burleigh WA-1650, 60 MHz resolution and 100 MHz accuracy). The wavemeter accuracy being limited to $3 \times 10^{-3}\text{ cm}^{-1}$, the absolute calibration was obtained by using reference line positions of methane obtained either from the HITRAN database [18] or from a high sensitivity FTS spectrum recently recorded in Reims ($l = 1603\text{ m}$, $P = 1$ and 5 Torr) [22]. The precision of the obtained wavenumber calibration estimated from the dispersion of the wavenumber differences is $1 \times 10^{-3}\text{ cm}^{-1}$. Each LNT spectrum was then calibrated by statistically matching the line positions to those of the corresponding RT spectrum.

Fig. 2 shows an overview comparison of the CW-CRDS spectra for the whole transparency window at RT and LNT temperature. The achieved sensitivity reveals the considerable spectral congestion of the spectra and the dramatic change induced by cooling, in particular in the low energy region of the investigated spectrum.

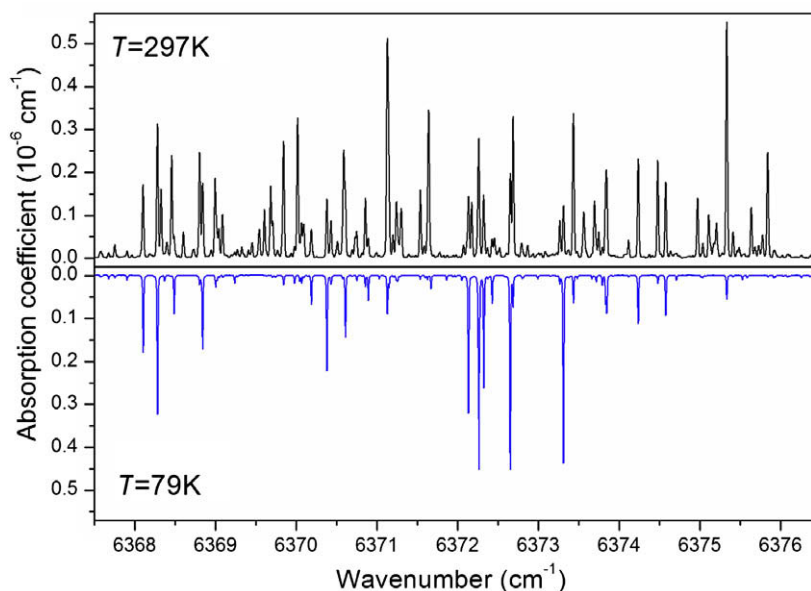


Fig. 3. Comparison of the CW-CRDS spectra of methane recorded at room temperature (upper panel) and liquid nitrogen room temperature (lower panel) near 6372 cm^{-1} .

The comparison around 6372 cm^{-1} presented in Fig. 3, illustrates the important variation of the line intensities leading to a LNT spectrum which is hardly recognizable compared to the RT spectrum. Even if the reduction of the rotational congestion is not impressive in Fig. 2, the density of lines is reduced and some spectral intervals appear free of absorption lines at LNT which is hardly the case at RT. The “fractal” appearance of the RT spectrum was illustrated in Ref. [9].

3. Construction of the line lists

The line intensity, S_{v_0} ($\text{cm}/\text{molecule}$), of a rovibrational transition centered at ν_0 , was obtained from the integrated absorption coefficient, A_{v_0} ($\text{cm}^{-2}/\text{molecule}$):

$$A_{v_0}(T) = \int_{\text{line}} \alpha_{\nu} d\nu = S_{v_0}(T)N \quad (1)$$

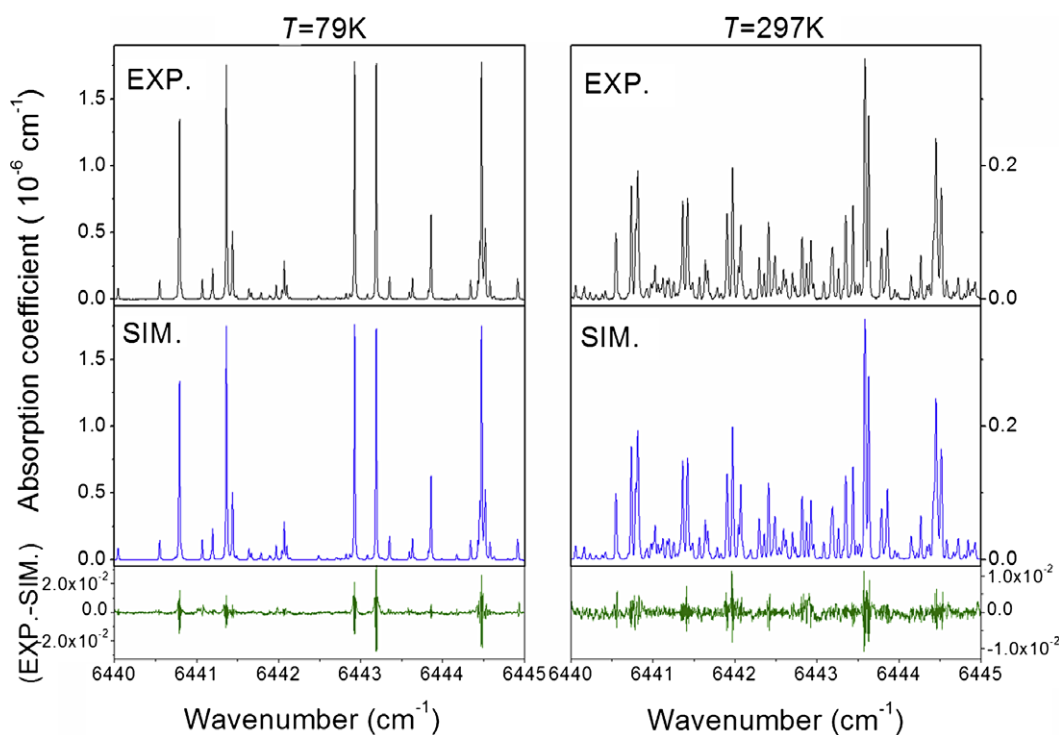


Fig. 4. An example of simulation of the CH_4 spectrum recorded at LNT (left hand) and RT (right hand) near 6442 cm^{-1} . From top to bottom: Upper panel: Experimental spectrum at LNT ($P = 9.02\text{ Torr}$) and RT ($P = 10.69\text{ Torr}$). Middle panel: Simulated spectrum resulting from the line fitting procedure (a Voigt profile was affected to each line). Lower panel: Residuals between the simulated and experimental spectra.

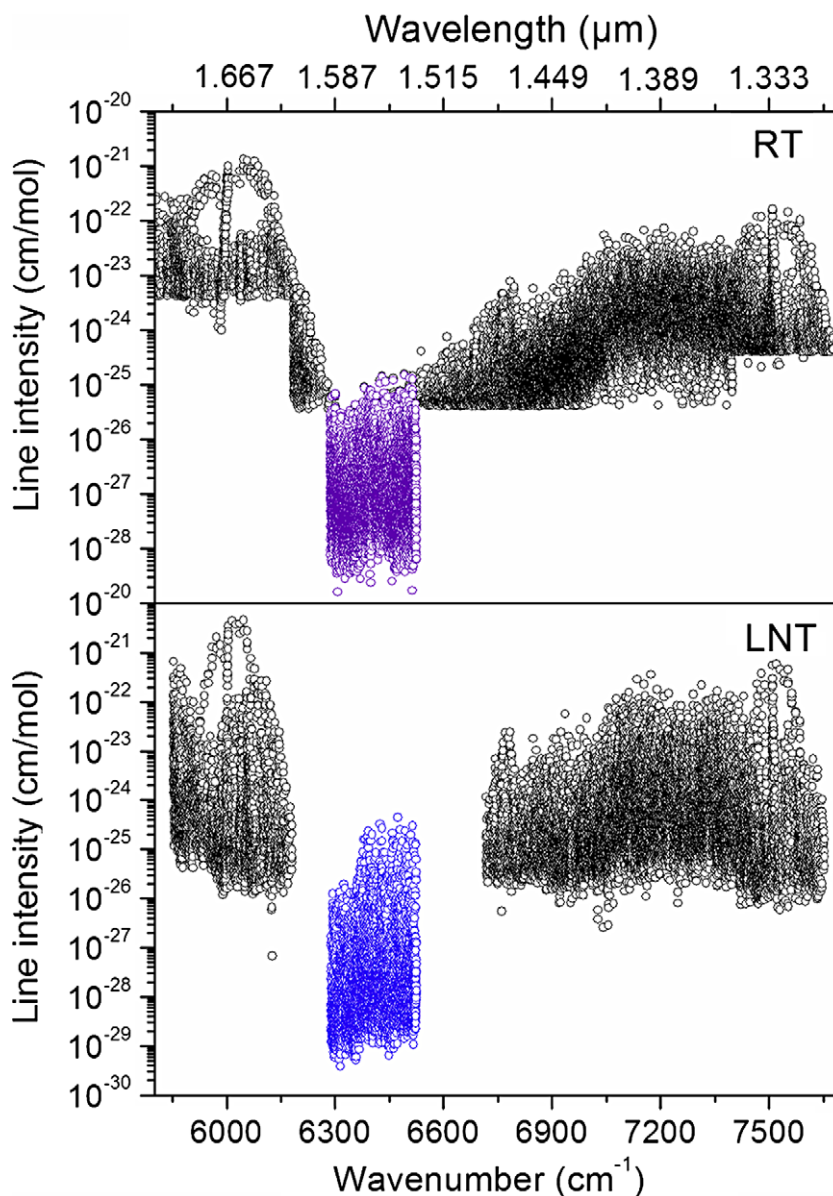


Fig. 5. Overview spectrum of methane between 5850 and 7700 cm^{-1} at RT (upper panel) and LNT (lower panel). The RT spectrum was obtained by gathering the HITRAN line list with the CW-CRDS line list presently obtained in the 6289–6526 cm^{-1} region. The LNT spectrum includes the line lists attached to Refs. [5,7] for the high energy part of the tetradecad and the icosad, respectively, together with the present CW-CRDS line list in the transparency window.

where ν is the wavenumber in cm^{-1} , $\alpha(\nu)$ is the absorption coefficient in cm^{-1} , and N is the molecular concentration in molecule/ cm^3 obtained from the measured pressure value: $P = NkT$.

The mode by mode scheme adopted for the acquisition of the CRDS spectra at LNT [8], leads to a reduced number of data points defining each line profile: the full profile is described by about six points separated by exactly 106 MHz corresponding to the Free Spectral Range of the CRDS cavity. This reduced number of data points does not prevent for a satisfactory fitting of the profile as it is compensated by the extreme precision on the corresponding frequencies allowed by the mode by mode data acquisition.

An interactive multi-line fitting program was used to reproduce the spectrum [23]. The first step of the spectrum analysis consisted in the manual determination of the spectral sections of overlapping or nearby transitions that could be fitted independently. It is worth underlining that as a general rule, lines are blended and isolated lines are exceptions in the RT spectrum. This is why the line profile fitting was performed first for the LNT spectrum which benefits from the reduction by a factor of 2 of the Doppler line width allow-

ing for the resolution of a number of multiplets which are strongly blended at room temperature. Even if a multispectrum treatment of the RT and LNT spectra was not undertaken, the LNT line list was of a great help for the fitting of the RT spectrum.

A Voigt function of the wavenumber was adopted for the line profile as the pressure self broadening has a significant contribution in particular at LNT: at 79 K and 10 Torr, the self broadening (HWHM $2.6 \times 10^{-3} \text{ cm}^{-1}$ [24]) is about half the Doppler broadening (HWHM $5.0 \times 10^{-3} \text{ cm}^{-1}$). The local baseline (assumed to be a cubic function of the wavenumber) and the three parameters of each Voigt profile (line center, integrated absorption coefficient, HWHM of the Lorentzian component) were fitted. The HWHM of the Gaussian component was fixed to its theoretical value for $^{12}\text{CH}_4$. In the case of blended lines or lines with low signal to noise ratios, the Lorentzian HWHM was also constrained to the average value obtained from nearby isolated lines.

The high density and the overlapping of the lines made the fitting of the spectrum a tremendous task: the average density of lines is more than 19 and 29 per cm^{-1} at LNT and RT, respectively.

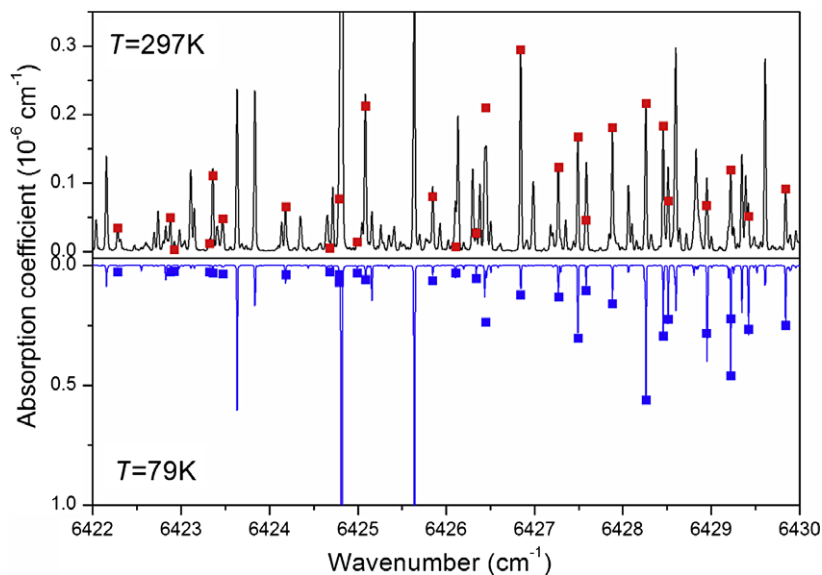


Fig. 6. Comparison of the CW-CRDS spectra of methane recorded at room temperature (upper panel) and liquid nitrogen room temperature (lower panel) in the region of the Q branch of the $3\nu_2$ band of CH_3D . The squares mark the transitions of the $3\nu_2$ band of CH_3D as provided in the HITRAN database [18]. The line intensities at 79 K have been calculated using the lower state energy values [18]. The intensity scale (right hand) has been adjusted to match the CW-CRDS absorption coefficients.

Fig. 4 shows an example of comparison between the measured and fitted spectra. Some significant differences between the observed and simulated spectra are still noted. They are probably due to the small sections of warm gas lying between the ends of the cold jacket and the supermirrors.

The achieved noise equivalent absorption corresponds to a minimum value on the order of 6×10^{-30} and 6×10^{-29} cm/molecule for the line intensities at 10 Torr pressure, at LNT and RT, respectively. This difference is due to the fact that at a given pressure, the peak depths in the LNT spectra are increased by nearly one order of magnitude as the Doppler widths are reduced by a factor of about 2 and the molecular concentration is about four times larger at LNT than at RT.

The complete line lists at RT and LNT were obtained by gathering the line lists corresponding to the different DFB laser diodes. The final RT dataset consists of 6868 lines with intensity values ranging from about 1.6×10^{-29} to 1.5×10^{-25} cm/molecule for methane in natural abundance at 297 K. The LNT line list consists of 4555 lines with intensity values ranging from about 3.9×10^{-30} to 4.5×10^{-25} cm/molecule at 79.3 K. The overview of the two line lists is included in Fig. 5.

4. Identification of the CH_3D transitions

Practically all the $3\nu_2$ transitions of CH_3D included in the HITRAN list could be identified in the RT CRDS spectra of methane in natural abundance. Fig. 6 shows the comparison of the CRDS spectra at LNT and RT in the region of the Q branch of the $3\nu_2$ band. The plots show the very good agreement with the corresponding HITRAN line list [18] – the intensities at 79.3 K were computed using the lower state energy values as given in HITRAN.

The $3\nu_2$ band of CH_3D provides the opportunity to determine the rotational temperature of methane in our sample. As mentioned above, a gas temperature of $T = 82.6$ K was obtained from the Doppler line profile analysis [8] in close agreement with the 81 K value previously determined by the same method from DAS spectra in the tetradecad region [3]. We did not try to use the $2\nu_3$ and $\nu_2 + 2\nu_3$ bands of $^{12}\text{CH}_4$ to derive the rotational temperature because they show highly blended multiplets for which accurate line intensities are difficult to derive. In spite of their

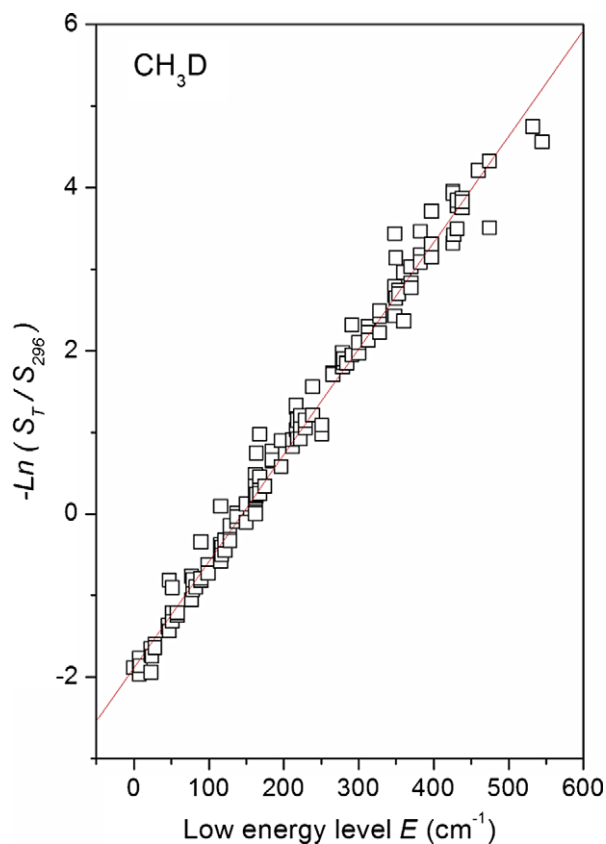


Fig. 7. Variation of the quantity $-\ln\left(\frac{S_{T_1}(T)}{S_{T_1}(T_0)}\right)$ versus the lower state energies of the transitions of $3\nu_2$ band of CH_3D . The best fit of the experimental data leads to a value of 79.3(4) K for the rotational temperature.

weakness in the CRDS spectrum of methane, the transitions of the $3\nu_2$ band of CH_3D are more suitable to evaluate the rotational temperature.

The temperature dependence of the line strengths is proportional to the Boltzmann factor [3,4]:

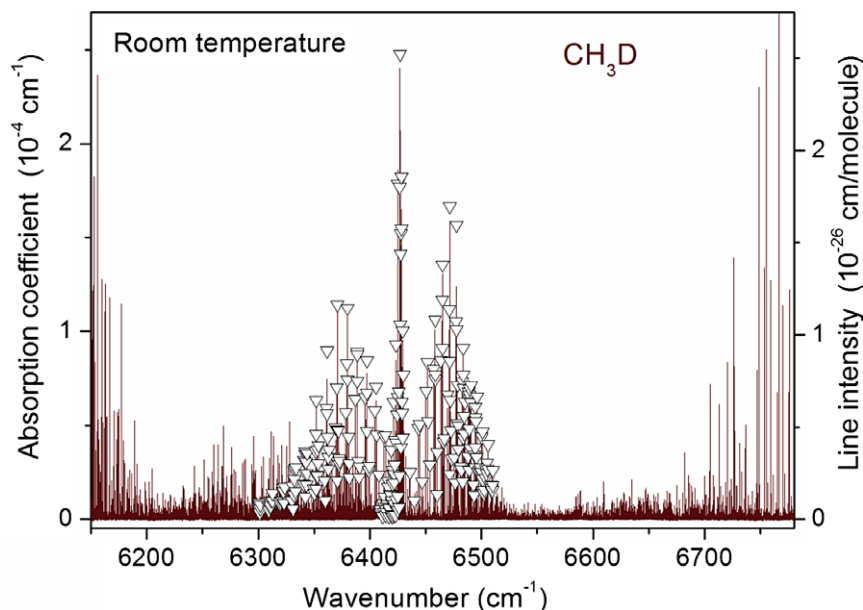


Fig. 8. Overview spectrum of CH_3D at room temperature recorded by Fourier Transform Spectroscopy between 6150 and 6780 cm^{-1} . The triangles marks the transitions of the $3\nu_2$ band of CH_3D as provided in the HITRAN database. The intensity scale (right hand) has been adjusted to match the FTS spectrum.

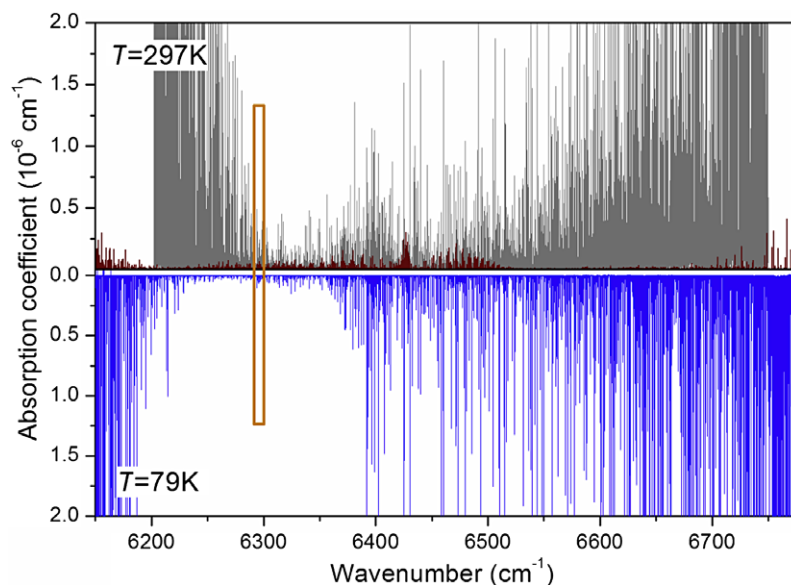


Fig. 9. Contribution of the CH_3D isotopologue to the methane absorption in the $1.58\text{ }\mu\text{m}$ transparency window of methane: Upper panel: Room temperature: the FTS spectrum of CH_3D has been superimposed to the CW-CRDS spectrum of methane, the ordinate scales have been chosen in order to match the absorption coefficients of the $3\nu_2$ band of CH_3D in the two spectra. Lower panel: CW-CRDS spectrum of methane at low temperature (79 K). The rectangle corresponds to the spectral region expanded in Fig. 10.

$$S_T(T) \propto \frac{\exp(-E/k_B T)}{Z(T)} \quad (2)$$

where $Z(T)$ is the partition function and E is the lower state energy level. In our temperature range, the vibrational excitation is negligible and only the rotational partition function has to be considered. $Z(T)$ being proportional to $T^{3/2}$, it leads to a simple expression for the ratio of line strengths at RT and LNT:

$$-\ln\left(\frac{S_{\nu_0}(T_1)}{S_{\nu_0}(T_0)}\right) = \frac{3}{2} \ln\left(\frac{T_1}{T_0}\right) + E\left[\frac{1}{kT_1} - \frac{1}{kT_0}\right] \quad (3)$$

where T_0 and T_1 are the RT and LNT, respectively.

One hundred and thirty-nine transitions of the $3\nu_2$ band were found in common in the RT and LNT line lists. The linear dependence of the quantity $-\ln\left(\frac{S_{\nu_0}(T_1)}{S_{\nu_0}(T_0)}\right)$ versus the values of the lower state energies provided in the HITRAN database is illustrated in Fig. 7. A value of $79.3(4)\text{ K}$ was derived for T_1 from the fit of the experimental values (Eq. (3)), the RT value being fixed to 297 K . The agreement between the obtained rotational temperature and the previous determination from the Doppler broadening (82.6 K [8]) is then satisfactory.

The smallest intensity values included in the HITRAN list for the $3\nu_2$ band of CH_3D are on the order of $4.0 \times 10^{-27}\text{ cm/molecule}$ (see Fig. 1), i.e. about two orders of magnitude above the sensitivity of our spectra. This is the reason why, in order to identify the numer-

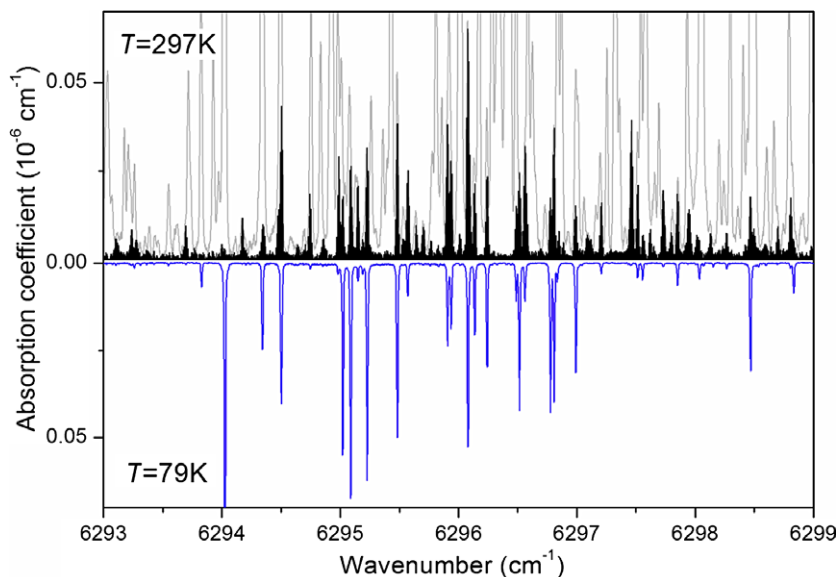


Fig. 10. Same as Fig. 9 for an expanded region around 6296 cm^{-1} . Most of the lines observed in the CW-CRDS spectrum of methane at low temperature (lower panel) are due to CH_3D in natural abundance as demonstrated by the comparison with the FTS spectrum of CH_3D at room temperature (upper panel). The CW-CRDS spectrum of methane displayed as background (light gray) in the upper panel shows that, at room temperature, the CH_3D transitions are completely obscured by much stronger CH_4 transitions.

ous CH_3D transitions observed in the CRDS spectra but missing in the HITRAN list, the spectrum of CH_3D was recorded separately by Fourier Transform Spectroscopy at USTC (Hefei, China).

The enriched CH_3D methane sample was purchased from Aldrich with a stated purity of 99%. The spectra in the $1\text{--}2\text{ }\mu\text{m}$ region were recorded with a Bruker IFS 120HR interferometer with a path length adjustable multi-path gas cell at room temperature. The unapodized resolution was 0.015 cm^{-1} . The recordings were performed using several absorption path lengths (15, 33 and 51 m) and pressure values (4.17 and 19.92 Torr). A tungsten source, a Ge detector and a CaF_2 beam-splitter were used. The gas sample pressure was measured using a capacitance manometer (MKS 627B) of 20 Torr full-scale range with accuracy of 0.15%. The line positions were calibrated using those of H_2O listed in the HITRAN database [18]. The accuracy of the centers of the unblended not-very-weak lines is estimated to be better than 0.001 cm^{-1} .

The overview of the FTS spectrum at RT reveals a high number of additional lines compared to HITRAN (Fig. 8). On the basis of this spectrum, the CH_3D transitions were discriminated in the CRDS spectra of methane at RT. In Fig. 9, we have superimposed to the RT CRDS spectrum of methane, the FTS spectrum of CH_3D with intensities scaled in order to match the intensities of the $3\nu_2$ band. Considering the congestion of the CH_3D (FTS) and methane (CRDS) spectra, both the positions and intensities had to be used as criteria to unambiguously identify the CH_3D lines in the CRDS spectrum. Finally, among the 6868 transitions observed at RT, 1282 were attributed to CH_3D . Obviously part of the CH_3D transitions are overlapping with CH_4 transitions. In the global line lists attached as Supplementary Material, the CH_3D transitions are indicated together with the CH_4 transitions which are believed to be strongly blended with CH_3D lines.

The identification of the CH_3D transitions in the LNT spectrum was more difficult as the intensity criterion could not be used as a result of the considerable variation of the intensities of the CH_3D transitions between RT and LNT. Hopefully, the reduced congestion of the LNT spectrum helped to discriminate the CH_3D lines using only the line position coincidence as criterion. As a rule, we decided that if the difference, δ , of the centers of lines observed at RT and LNT differ by less than 0.002 cm^{-1} , the two lines correspond to the same transition and then to the same species. In other

words, we transferred the species determination from the RT spectrum to the LNT spectrum. Nearly 60% of the very weak lines observed at LNT but unobserved at RT were left without isotopologue determination. They represent only 8.2% of the total absorbance at LNT.

A consistent calibration of the different line lists and spectra is a prerequisite of the above treatment and also for the application of the “two temperature method” (see next section). During the analysis, an inconsistency on the order of 0.003 cm^{-1} was evidenced between the CH_4 and CH_3D line positions provided in HITRAN. In our region, only 73 transitions are included in the HITRAN line list of CH_4 . They are on average $1.1 \times 10^{-3}\text{ cm}^{-1}$ above our values while the HITRAN positions for CH_3D are on average $1.8 \times 10^{-3}\text{ cm}^{-1}$ below our values.

Finally, among the 6868 and 4555 transitions measured at RT and LNT, respectively, 1282 and 536 were identified as CH_3D transitions. They represent 7.0% and 9.9% of the total absorbance in the region at RT and LNT, respectively.

An important observation is that, in the region around 6300 cm^{-1} , the CH_3D absorption lines observed at LNT are strongly dominating. As an example, Fig. 10 shows an enlargement of the spectrum of Fig. 9 around 6296 cm^{-1} . While the CH_3D transitions are obscured by much stronger CH_4 lines in the RT spectrum, they are dominating the LNT spectrum.

It is worth mentioning that among the CH_4 lines observed in our spectra, we could not discriminate the $^{12}\text{CH}_4$ and $^{13}\text{CH}_4$ transitions. The calculated ($^{12}\text{CH}_4\text{--}^{13}\text{CH}_4$) isotopic shifts of the $5\nu_4$ and $\nu_2 + 4\nu_4$ bands being -38 cm^{-1} and -29 cm^{-1} [25], respectively, the $^{13}\text{CH}_4$ relative contribution to the absorbance in the region, may exceed the 1.1% relative abundance of this isotopologue. In the line lists attached as Supplementary Material, the $^{12}\text{CH}_4$ and $^{13}\text{CH}_4$ transitions are both marked with “H” while “D” corresponds to the CH_3D species.

5. Determination of the lower state energy

In the high absorbing regions surrounding the presently studied transparency window, we have systematically used the ratio of the line intensities measured at LNT and RT to determine the low energy levels of the transitions in common in the two spectra

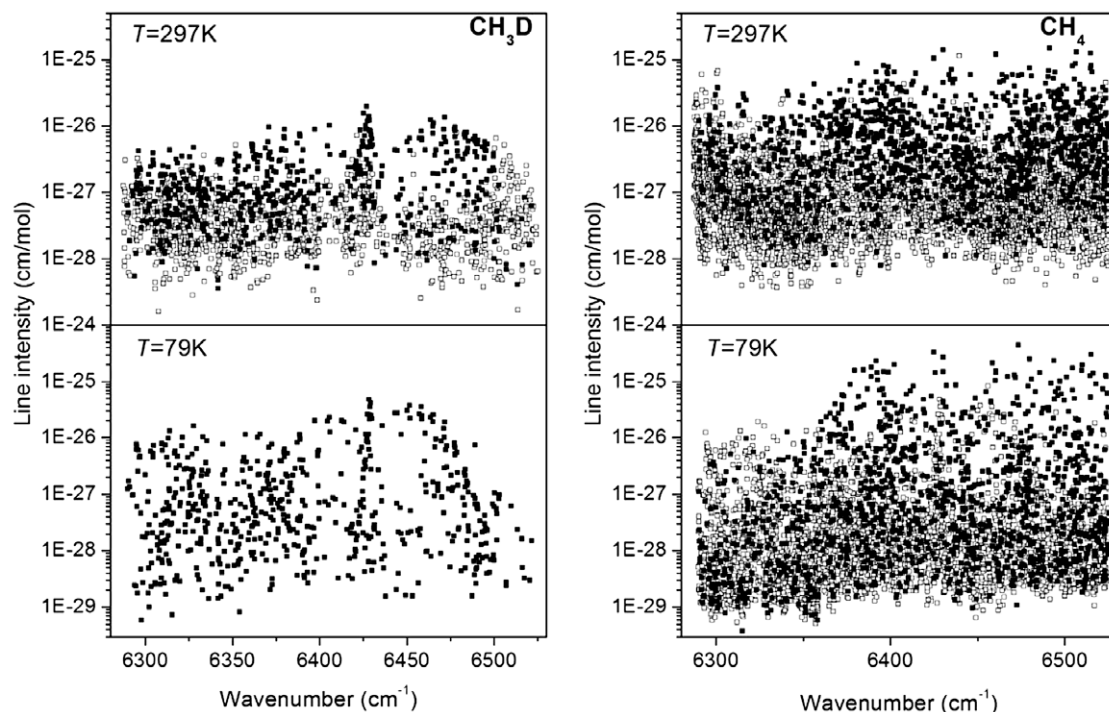


Fig. 11. Overview of the spectrum of CH_3D (left hand) and CH_4 (right hand) between 6289 and 6526 cm^{-1} region as obtained from the analysis of the CW-CRDS spectra at 297 K (upper panel) and 79 K (lower panel). The filled symbols highlight the CH_4 and CH_3D transitions for which the low energy value was derived from the ratio of the line intensities ($\delta < 0.002 \text{ cm}^{-1}$).

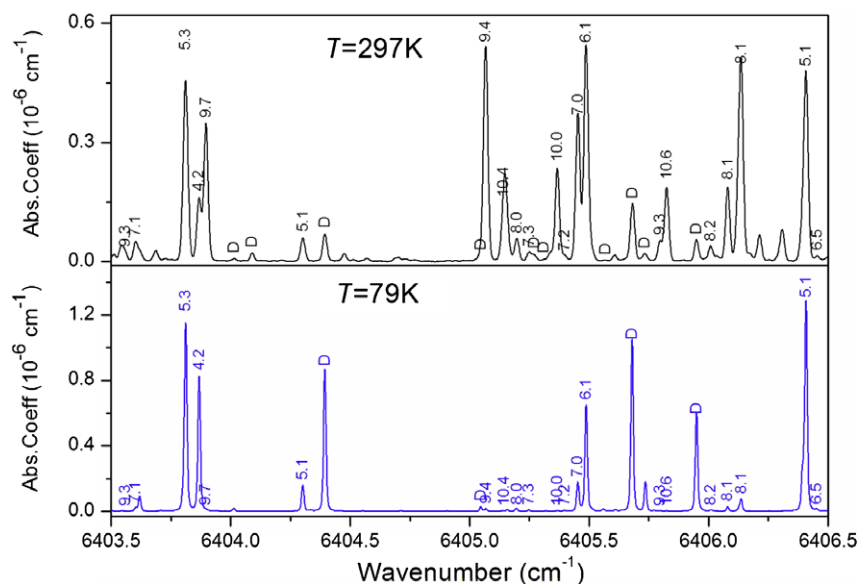


Fig. 12. Comparison of the CW-CRDS spectra of methane at liquid nitrogen temperature (lower panel) and room temperature (upper panel) near 6405 cm^{-1} . The RT and LNT spectra were recorded with pressures of 10 and 5 Torr, respectively. The CH_3D transitions are marked with “D”. The J values obtained from the temperature variation of the line intensities are indicated for the CH_4 isotopologue.

[3–7]. This “two temperature method” proved to be robust and reliable to account for the temperature dependence of the methane absorption. Taking into account the partition function, the lower energy can be calculated using Eq. (3) which can be rewritten:

$$\ln \left(\frac{S_{\nu_0}(T_1)T_1^{3/2}}{S_{\nu_0}(T_0)T_0^{3/2}} \right) = E \left[\frac{1}{kT_0} - \frac{1}{kT_1} \right] \quad (4)$$

where T_0 and T_1 are the RT and the LNT, respectively.

The above expression is based on the assumption that the rotational partition function $Z(T)$ follows a $T^{3/2}$ temperature dependence. In the LNT–RT range, this approximation holds within 3% for both CH_4 and CH_3D [18] and the two temperature method can be applied independently of the species.

The automatic association of the lines of the RT and LNT datasets uses as only criterion the coincidence of their centers. The importance of the quality of the wavenumber calibration of the spectra and of the precision on the line center determinations has been

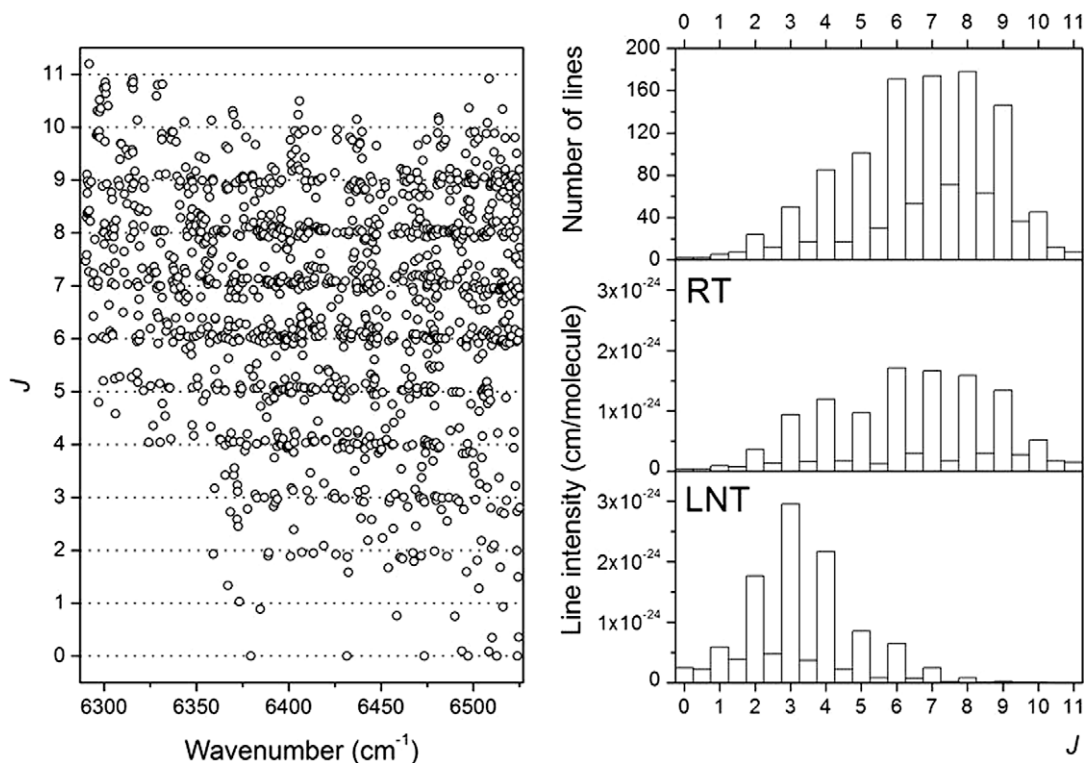


Fig. 13. Left hand: Empirical J values of the CH_4 transitions observed between 6289 and 6526 cm^{-1} versus the transition wavenumber. Right hand: Histograms of the empirical J values determined for the CH_4 transitions (step interval of 0.5). The upper panel shows the number of lines while, in the two lower panels, the corresponding RT and LNT line intensities were added for each step interval. Note that the contrast between integers and non-integers is more pronounced in terms of intensities than in terms of number of lines (see text).

Table 1
Wavenumbers and line strengths of the methane transitions measured at 79.3 K by CW-Cavity Ring Down Spectroscopy near 6393 cm^{-1} . This table is a small section of the list of 4555 transitions between 6289 and 6526 cm^{-1} which is provided as [Supplementary Material](#).

ISO ^a	$T = 79.3 \text{ K}$		$T = 297 \text{ K}$		$E \text{ (cm}^{-1}\text{)}$	J
	Center (cm^{-1})	Intensity (cm/mol)	Center (cm^{-1})	Intensity (cm/mol)		
H	6392.6255	7.209E–29	6392.6256	6.718E–27	489.90	9.18
D	6392.6655	2.149E–27	6392.6666	7.680E–28	71.56	
H	6392.7182	1.038E–25	6392.7182	3.158E–26	59.46	2.91
	6392.8648	2.641E–28				
	6393.0169	3.074E–29				
H	6393.0311	1.750E–28	6393.0297	3.376E–28	198.34	5.67
	6393.0524	9.479E–29				
D	6393.1169	4.056E–29	6393.1177	1.319E–28	237.61	
	6393.1327	1.544E–28				
D	6393.1482	2.604E–29	6393.1463	6.887E–28	395.20	
H	6393.1975	6.867E–29	6393.1974	4.612E–28	292.14	6.98
H	6393.2825	3.554E–28	6393.2850	1.400E–26	425.16*	8.52
H	6393.2875	4.343E–28	6393.2850	1.400E–26	410.09*	8.36
	6393.4135	5.226E–29				
	6393.5520	1.973E–28				
H	6393.5961	1.508E–26	6393.5958	1.718E–26	158.74	5.03
H	6393.6876	2.857E–27	6393.6871	7.185E–27	218.28	5.97
H	6393.7041	2.269E–27	6393.7029	1.458E–27	115.68	4.23
H	6393.7800	6.948E–26	6393.7795	3.767E–26	102.91	3.96
D	6393.8287	1.581E–28	6393.8280	1.887E–28	162.24	
H	6393.8692	4.016E–26	6393.8689	1.261E–26	61.83	2.97
H	6394.0647	5.332E–28	6394.0639	4.169E–27	303.57	7.13
H	6394.1002	1.899E–26	6394.0998	2.137E–26	157.81	5.01
H	6394.1151	1.519E–27	6394.1179	1.977E–27	168.75*	5.20
	6394.1313	5.415E–29				
H	6394.1533	9.937E–28	6394.1525	7.268E–27	298.55	7.06
D	6394.2465	1.382E–28	6394.2457	9.793E–28	296.17	

The low energy values, E , were obtained for the transitions whose center coincides with that of a line observed in the 297 K spectrum ($\delta < 0.002 \text{ cm}^{-1}$). The “*” symbol in the last column marks the lines whose RT and LNT line centers differ by $0.002 < \delta < 0.003 \text{ cm}^{-1}$.

For CH_4 , the empirical J values are given in the last column.

^a Isotopologue: “H” corresponds to both the $^{12}\text{CH}_4$ and $^{13}\text{CH}_4$ isotopologues while “D” corresponds to CH_3D (see text).

underlined and discussed in details in Ref. [7]. Indeed a strict criterion is chosen to insure that a RT line and a LNT line correspond to the same transition: the difference, δ , of their line centers must differ by less than 0.002 cm^{-1} . This value which takes into account the average uncertainties on the two line center determinations corresponds to one-fifth and one tenth of the Doppler width (FWHM) at LNT and RT, respectively. According to this criterion, 1327 and 536 pairs of transitions were found in coincidence for CH_4 and CH_3D , respectively. They are highlighted in the overview plots presented in Fig. 11. Overall, the associated transitions represent 65.4% and 91.8% of the total absorbance at RT and LNT, respectively.

Using Eq. (4), the lower energy values, E , were empirically determined for both isotopologues. The CH_3D isotopologue being a symmetric top molecule, the values of the rotational levels are too dense to unambiguously derive empirical values of the J and K quantum numbers from the E value. In the case of both $^{12}\text{CH}_4$ and $^{13}\text{CH}_4$, the rotational energy levels are well separated and the corresponding empirical J values can be computed from $J_{\text{emp}} = \sqrt{\frac{1}{4} + \frac{E}{B_0}} - \frac{1}{2}$ where $B_0 = 5.214 \text{ cm}^{-1}$ is the $^{12}\text{CH}_4$ (and $^{13}\text{CH}_4$) ground state rotational constant. The above expression based on a simple rigid rotor approximation is sufficient as the splitting of the tetrahedral multiplets remains small in our range of J values (for instance 0.5 cm^{-1} at $J = 12$). As an example, the CH_3D transitions and the obtained empirical J values of the CH_4 transitions are indicated on the RT and LNT spectra displayed in Fig. 12.

In Fig. 13, the empirical J values are plotted versus the CH_4 line centers. The observed propensity of the J values to be close to integers is a clear indication of the validity of the method as confirmed by the histograms also included in this figure. The contrast between integer and non-integer J values is more pronounced in terms of intensities than in terms of number of lines (Fig. 13, right hand). This is due to the fact that the uncertainty on the line intensities values (and then on the J values) is larger for the weaker lines and then, on average, non-integer J values correspond to smaller intensities. At both 79 and 297 K, 75.6% of the J determinations lead to J values falling within a ± 0.25 interval around integer values. The corresponding transitions bring 85.0% of the absorbance of the CH_4 lines with J determinations. Our previous studies [4–7] showed that the $\delta < 0.002 \text{ cm}^{-1}$ criterion is too strict in the case of strongly blended or very weak lines and that additional pairs of lines correspond undoubtedly to the same transitions and should be associated. We decided to increase δ_{Max} up to 0.003 cm^{-1} which allowed deriving 301 additional low energy determinations representing 2.1% of the total absorbance at LNT. The derived low energy values of the lines with $0.002 < \delta < 0.003 \text{ cm}^{-1}$ are expected to be less accurate. They are specifically marked in the line lists provided as [Supplementary Material](#). The complete sets of transitions measured at 79.3 and 297 K are provided as two separate line lists including the species identification, the E values of the lower state for the pairs of associated transitions, together with the empirical J values in the case of the CH_4 isotopologue. Table 1 gives a sample of the low temperature line list.

6. Conclusion

With the help of a specifically designed cryogenic cell and a mode by mode data acquisition of the CW-CRDS spectrum, the absorption spectrum of methane in the $1.58 \mu\text{m}$ transparency window has been characterized for the first time at low temperature. The sensitivity achieved at both RT and LNT ($\alpha_{\text{min}} \sim 3 \times 10^{-10} \text{ cm}^{-1}$) lowers by more than three orders of magnitude the one we achieved by differential absorption spectroscopy in the nearby strong absorbing regions. Line intensities as weak as $10^{-29} \text{ cm}^2/\text{molecule}$ could be measured.

The cooling down to LNT induces important changes in the appearance of the spectra: the reduction of the rotational congestion leads to an enlargement of the transparency windows. This effect is particularly marked in the low energy part of the window: the numerous high rotational transitions of the R branches of the high energy bands of the tetradecad have their intensities drastically reduced and practically vanish at LNT – for instance, the intensity of a transition from a $J = 11$ level is decreased by three orders of magnitude when cooling down to 79.3 K. Most of the residual absorption lines observed in the LNT spectrum around 6300 cm^{-1} are underlying transitions of CH_3D in natural abundance which are mostly obscured by the CH_4 absorption at RT.

The positions and strengths of 6868 and 4555 transitions were obtained from the analysis of the absorption spectra at RT and LNT, respectively. On the basis of a spectrum of CH_3D recorded separately by FTS, the CH_3D lines could be discriminated. This identification of the contribution of the CH_3D lines in the residual absorption at LNT is an important result with implication in planetary science as it will allow us to take into account the variation of the D/H ratio of the different solar system objects. For instance, the D/H abundance for Saturn and Jupiter is about 10 times lower than for Titan, Neptune or our Earth. An accurate description of the transmission in the considered transparency window will then require scaling the CH_3D intensities according to the $\text{CH}_3\text{D}/\text{CH}_4$ relative abundance of the considered objects.

On the basis of line positions coincidence, $\delta < 0.003 \text{ cm}^{-1}$, a total of 640 CH_3D and 1524 CH_4 transitions were found in common in the RT and LNT line lists. Empirical low energy values of the lower level of these transitions could be determined from the variation of the line intensities. They are given in the exhaustive line lists provided as [Supplementary Material](#) which can be used to account accurately for the temperature dependence of the methane absorption in the region. Of particular interest for future theoretical developments, the construction of the CH_4 line list with empirical lower J values will help for the modeling of the eight components of the $5\nu_4$ band, which is the lowest energy band of the icosad.

Although the obtained results represent a first and important improvement of the knowledge of this transparency window, the analysis can be further extended. To identify the isotopologue species of the transitions observed only at LNT, the CW-CRDS spectrum of highly enriched CH_3D should be recorded at LNT. Then, the two temperature method could be applied to the RT and LNT lines of CH_3D measured from the FTS and CRDS spectrum, respectively. Note that in view of the absence of regularity and of the congestion of the CH_3D spectrum, a full rovibrational assignment of the transitions which do not belong to the $3\nu_2$ band seems out of reach in the near future and the two temperature method appears to be the most suitable alternative to account for the temperature dependence of the CH_3D absorption in the region.

An important work is also needed to complete the coverage of the transparency window (see Fig. 5). By combining the results previously obtained by differential absorption spectroscopy and presently by CW-CRDS, we hope that in a near future, we will be able to provide a complete line list at LNT and RT which will allow (i) calculating the temperature dependence of methane absorption over the whole $1.26\text{--}1.70 \mu\text{m}$ range and (ii) quantifying the importance of the CH_3D contribution in the $1.58 \mu\text{m}$ transparency window. These results will directly feed into radiative transfer codes applied to the modeling of the methane opacity on Titan and the giant planets.

Acknowledgments

This work is part of the ANR project “CH4@Titan” (ref. BLAN08-2_321467) which is a joint effort among four French laboratories (ICB-Dijon, GSMA-Reims, LSP-Grenoble and LESIA-Meudon) to ade-

quately model the methane opacity. We thank the GSMA group (Reims, France) for providing us with their long path absorption spectrum of methane which was used to refine the wavenumber calibration of the CRDS spectra. The support of the Groupement de Recherche International SAMIA between CNRS (France), RFBR (Russia) and CAS (China) is acknowledged.

Appendix A. Supplementary data

Supplementary data for this article are available on ScienceDirect (www.sciencedirect.com) and as part of the Ohio State University Molecular Spectroscopy Archives (http://library.osu.edu/sites/msa/jmsa_hp.htm).

References

- [1] P.G.J. Irwin, K. Sihra, N. Bowles, F.W. Taylor, S.B. Calcutt, *Icarus* 176 (2005) 255–271.
- [2] A. Negrão, A. Coustenis, E. Lellouch, J.-P. Maillard, P. Rannou, B. Schmitt, C.P. McKay, V. Boudon, *Planet. Space Sci.* 54 (2006) 1225–1246.
- [3] S. Kassı, B. Gao, D. Romanini, A. Campargue, *Phys. Chem. Chem. Phys.* 10 (2008) 4410–4419.
- [4] B. Gao, S. Kassı, A. Campargue, *J. Mol. Spectrosc.* 253 (2009) 55–63.
- [5] Le Wang, S. Kassı, A. Campargue, *J. Quant. Spectrosc. Radiat. Transfer*, in press. doi: 10.1016/j.jqsrt.2009.10.019.
- [6] E. Sciamma-O'Brien, S. Kassı, B. Gao, A. Campargue, *J. Quant. Spectrosc. Radiat. Transfer* 110 (2009) 951–963.
- [7] A. Campargue, Le Wang, S. Kassı, M. Mašát, O. Votava, *J. Quant. Spectrosc. Radiat. Transfer*, in press. doi: 10.1016/j.jqsrt.2009.11.025.
- [8] S. Kassı, D. Romanini, A. Campargue, *Chem. Phys. Lett.* 477 (2009) 17–21.
- [9] A.W. Liu, S. Kassı, A. Campargue, *Chem. Phys. Lett.* 447 (2007) 16–20.
- [10] C. de Bergh, B.L. Lutz, T. Owen, J. Brault, J. Chauville, *Astrophys. J.* 311 (1986) 501–510.
- [11] C. de Bergh, B.L. Lutz, T. Owen, J. Chauville, *Astrophys. J.* 329 (1988) 951–955.
- [12] C. de Bergh, B.L. Lutz, T. Owen, J.P. Maillard, *Astrophys. J.* 355 (1990) 661–666.
- [13] P.F. Penteadó, C.A. Griffith, T.K. Greathouse, C. de Bergh, *Astrophys. J.* 629 (2005) L53–L56.
- [14] B.L. Lutz, C. de Bergh, J.P. Maillard, *Astrophys. J.* 273 (1983) 397–408.
- [15] C. Boussin, B.L. Lutz, C. de Bergh, A. Hamdouni, *J. Quant. Spectrosc. Radiat. Transfer* 60 (1998) 501–514.
- [16] C. Boussin, B.L. Lutz, A. Hamdouni, C. de Bergh, *J. Quant. Spectrosc. Radiat. Transfer* 63 (1999) 49–84.
- [17] J.J. Plateaux, L. Régalia, C. Boussin, A. Barbe, *J. Quant. Spectrosc. Radiat. Transfer* 68 (2001) 507–520.
- [18] L.S. Rothman, I.E. Gordon, A. Barbe, D.C. Benner, P.F. Bernath, et al., *J. Quant. Spectrosc. Radiat. Transfer* 110 (2009) 533–572.
- [19] J. Bowman, T. Carrington, H.-D. Meyer, *Mol. Phys.* 106 (2008) 2145–2182.
- [20] J. Morville, D. Romanini, A.A. Kachanov, M. Chenevier, *Appl. Phys. D* 78 (2004) 465–476.
- [21] B.V. Perevalov, S. Kassı, D. Romanini, V.I. Perevalov, S.A. Tashkun, A. Campargue, *J. Mol. Spectrosc.* 238 (2006) 241–255.
- [22] X. Thomas, L. Régalia, L. Daumont, A. Nikitin, private communication.
- [23] L. Daumont, J. Vander Auwera, J.-L. Teffo, V.I. Perevalov, S.A. Tashkun, *J. Mol. Spectrosc.* 208 (2001) 281–291.
- [24] F. Ménard-Bourcin, J. Ménard, C. Boursier, *J. Mol. Spectrosc.* 242 (2007) 55–63.
- [25] A.V. Nikitin, S. Mikhailenko, I. Morino, T. Yokota, R. Kumazawa, T. Watanabe, *J. Quant. Spectrosc. Radiat. Transfer* 110 (2009) 964–973.